

# Thermo- and salt-responsive poly(NIPAm-co-AAc-Brij-58) microgels: adjustable size, stability under salt stimulus, and rapid protein adsorption/desorption

Yalong Liu<sup>1</sup> · Lijuan Xing<sup>1</sup> · Qingsong Zhang<sup>1,3</sup> · Qifeng Mu<sup>1</sup> · Pengfei Liu<sup>2</sup> · Kun Chen<sup>1</sup> · Li Chen<sup>1</sup> · Xiaoyong Zhang<sup>3</sup> · Ke Wang<sup>3</sup> · Yen Wei<sup>3</sup>

Received: 17 September 2015 / Revised: 5 December 2015 / Accepted: 6 December 2015 / Published online: 30 December 2015  
© Springer-Verlag Berlin Heidelberg 2015

**Abstract** Based on *N*-isopropylacrylamide (NIPAm) and modified copolymer of liquid crystal surfactant polyoxyethylene 20 cetyl ether (AAc-Brij-58), a series of “smart” poly(NIPAm-co-AAc-Brij-58) (ACM) microgels with controllable particle size and adjustable salt stability have been successfully fabricated by aqueous precipitation polymerization. The stability under the stimulus of salt and protein adsorption/desorption behavior of ACM microgels were explored. It can be found that when the mass percentage of AAc-Brij-58/NIPAm is 1 wt.%, the ACM01 microgel film presents the lowest contact angle (ca. 35.9°) and the highest hydrodynamic diameters ( $D_H$ ) value (ca. 1100 nm) with the increase of volume phase transition temperature (VPTT). In terms of transmittance change versus different concentrations of NaCl solution and transmittance versus temperature under certain salt concentrations, the responsibility of ACM microgel under ionic strength is investigated sufficiently. The adsorption/desorption behavior of ACM microgels to Bovine Serum Albumin (BSA) is also revealed. The results show that the maximum adsorption amount of AMC01 to BSA reaches 982.7

±26 mg/g at 25 °C, much higher than that of ACM0 (714.7 ±36 mg/g) and ACM02 microgels (402±20 mg/g).

**Keywords** Microgel · *N*-isopropylacrylamide · Sensitivity · Adsorption · Stability

## Introduction

Responsive microgels have been drawing extensive attention since 1986 because of their special structure, small particle size, and high specific surface area [1]. In recent years, smart microgels show promising prospect in the fields of controllable release of drug, protein adsorption and separation, photoelectric switch, and immobilization of enzyme [2–5], which make more and more researchers pay attention to them. There are many kinds of smart microgels such as thermosensitive [6–8], pH-sensitive [9], photo-sensitive microgels [10], and so on. By virtue of volume phase transition temperature (VPTT) around 32 °C and closeness to the normal temperature of the body, much more attention have been paid to the modification of poly(*N*-isopropylacrylamide) (PNIPAm) microgels [11]. In fact, lots of reviews related to stimuli-responsive PNIPAm-based microgels have been reported recently [12–14].

It has been recognized that within the numerous characteristics of “smart” microgels, the unstability of microgel dispersions under different concentrations of salt is very prominent. In the report of Gan et al. [15], the gelation of poly(*N*-isopropylacrylamide-co-2-hydroxyethyl methacrylate) microgel dispersions with ionic intensity increasing has been investigated. With the introduction of calcium chloride (CaCl<sub>2</sub>), cross-linked physical networks formed in the microgel dispersions. Meanwhile, they found that the gelation of the microgel dispersions was also affected by certain concentration of sodium chloride (NaCl). Sow et al. [16] investigated the effect of

✉ Qingsong Zhang  
zqs8011@163.com

✉ Yen Wei  
weiyen@tsinghua.edu.cn

<sup>1</sup> State Key Laboratory of Separation Membranes and Membrane Processes, School of Materials Science and Engineering, Tianjin Polytechnic University, Tianjin 300387, China

<sup>2</sup> School of Computer Science & Software Engineering, Tianjin Polytechnic University, Tianjin 300387, China

<sup>3</sup> Department of Chemistry, Tsinghua University, Beijing 100084, China

NaCl on the aggregation of nanosized fish gelatin. It was found that the addition of 1.5 % NaCl resulted in the formation of aggregates and the reduction of gel intensity. However, with the same concentration, sucrose affected the stability of fish gelatin less than NaCl did.

With the rapid development of biotechnology, protein adsorption and separation plays a highly significant role in it. Among the masses of practical applications of microgels, much attention has focused on the adsorption/desorption behavior of protein onto smart microgels. By free-radical precipitation polymerization, PNIPAm microgel particles cross-linked with different concentrations of poly(ethylene glycol) (PEG) diacrylates of three different PEG chain lengths were synthesized by Nolan et al. [17]. They proved that the adsorption of protein decreased obviously with the increase of PEG length and concentration. It can be attributed to the increased hydrophilicity of microgels. The adsorption behavior of human IgG onto thermo-sensitive poly(methyl methacrylate)/PNIPAm microgels upon different pH values and temperatures have been studied by Silva et al. [18]. They found that the adsorption behavior was intensely affected by temperature at pH = 9, while at pH = 5 it turned out to be that the maximum absorption mass was the same as that at 25 and 40 °C. Taking advantage of PEGylation technique, PNIPAm-co-PEGMA microgels were obtained by Trongsatitkul et al. [19]. It was found that the degree of PEGylation significantly affected the adsorption of bovine serum albumin (BSA) on the microgels surface.

Although PNIPAm-based microgels with good adsorption of BSA have been reported, the adsorption behaviors of PNIPAm-based microgel containing liquid crystal unit upon BSA are still unknown. In our previous work [20], via esterification between acrylic acid (AAc) and polyoxyethylene 20 cetyl ether (Brij-58), we successfully synthesized AAc-Brij-58, and prepared the corresponding bulk hydrogels. However, compared to the bulk hydrogels, microgels take great advantages over drug release and delivery in vivo and adsorption/desorption behavior. To reveal the relationship between microgel and stability under salt stimulus and rapid protein adsorption/desorption, a novel poly(NIPAm-co-AAc-Brij-58) microgel (ACM) with different mass percentages was designed and fabricated by precipitation polymerization [21, 22]. The chemical composition, appearance, and hydrophilic/hydrophobic properties of synthesized microgel were investigated by the methods of FTIR, TEM, and the contact angle meter. To clarify the thermo-sensitivity of obtained microgel latexes, dynamic light scattering (DLS), differential scanning calorimetry (DSC), and turbidity analysis were carried out jointly. The turbidity method was applied in order to explore the stability of microgels versus temperature and ion concentration. Furthermore, the adsorption/desorption behavior of BSA onto microgel was investigated and the comparison with corresponding bulk hydrogels was conducted.

## Experimental

### Materials

*N*-isopropylacrylamide (NIPAm, 95 %, Tokyo Kasei Kogyo Co.) was purified by repeated recrystallization in a mixture of toluene and hexane (60:40, *V/V*). Polyoxyethylene 20 cetyl ether (Brij-58) was purchased from Shanghai Meryer Chemical Technology Co., Ltd. Acrylic acid (AAc) was purchased from Tianjin Real & Lead Chemical Co., Ltd., China. Liquid crystal monomer C<sub>16</sub>H<sub>33</sub>(OCH<sub>2</sub>CH<sub>2</sub>)<sub>20</sub>O-COCH=CH<sub>2</sub> (hereinafter referred to as AAc-Brij-58) was prepared upon our previous report based on AAc and Brij-58 [20]. *N,N'*-methylenebisacrylamide (MBA, a cross-linker) was purchased from Tianjin Kemiou Chemical Reagent Co. and recrystallized by methanol. Initiator ammonium persulfate (APS) was obtained from Shanghai Chemical Reagent Co. and used without any purification. BSA (molecular weight 68,000) was purchased from Beijing Solarbio Science & Technology Co., China. Hydrophilic Durapore polyvinylidene fluoride (PVDF) filter membranes with the size of 50 mm × 0.22 μm were purchased from Shanghai Xinya Purifier Devices Factory. The greatest advantage of Durapore PVDF filter membranes is the ultra low protein adsorption (protein recovery reaches 99 %). The dialysis membrane (cutoff *M<sub>w</sub>* = 14, 000) was purchased from Beijing Solarbio science and technology company. The water used was Milli-Q grade. Other raw materials and reagents were all analytical pure and used as received.

### Synthesis of poly(NIPAm-co-AAc-Brij-58) microgels

The poly(NIPAm-co-AAc-Brij-58) microgels were synthesized by aqueous precipitation polymerization. In brief, the polymerizable monomer AAc-Brij-58 was firstly dissolved in 150 mL of deionized water under continuous stirring till the uniform solution formed. Then, 8.84 mmol of NIPAm monomer and 0.65 mmol MBA were added successively. After 30 min, the above mixtures were gradually heated to 70 °C under water bath and nitrogen stream. As the reaction temperature reaches equilibrium, 0.065 mmol of APS (dissolved in 1 mL of water) was added. The whole reaction lasted for 6 h at 70 °C under nitrogen atmosphere. At the beginning of the polymerization, the solution color changed from transparent to light blue in a few minutes, then slowly turned to a milky white. In the process of reaction, the pH value of solution remained at around 6–7. Finally, the poly(NIPAm-co-AAc-Brij-58) microgel latex was obtained.

The obtained latex was first filtered with pore size 10–15 μm filter paper removing the aggregates, and then the dispersion was purified with dialysis membrane in deionized water for 2 weeks to remove unreacted monomers and other

impurities. The subsequent products were represented as ACMX, here X represents the mass percentage of AAc-Brij-58/NIPAm, such as ACM02 means that the dosage of AAc-Brij-58 and NIPAm is 0.02 g and 1.0 g, respectively.

#### Fourier transform infrared spectroscopy (FTIR)

The ACM microgel solution was firstly freeze-dried in refrigerator at  $-20\text{ }^{\circ}\text{C}$  for 1 h. The completely frozen sample was freeze-dried at  $-60\text{ }^{\circ}\text{C}$  with freeze dryer (Alpha1-4LD, German Christ Inc.) subsequently for 5 h. The chemical composition was determined by FTIR (SENSOR 37, Germany) using a KBr tablet containing dried microgel powders.

#### Transmission electron microscope (TEM)

Firstly, the ACM microgel aqueous solution with concentration of 1 wt.% was prepared. Then a tiny AAc-Brij-58 solution was dropped onto a pure copper mesh before being air-dried at  $25\text{ }^{\circ}\text{C}$ . The TEM graphs were performed on a Hitachi (H-7650, Japan) transmission electron microscope.

#### Dynamic light scattering (DLS)

The hydrodynamic diameters ( $D_H$ ) and size distribution of ACM microgel were performed on DLS (Delsa™ Nano, Beckman Ltd, America) at  $28\sim 45\text{ }^{\circ}\text{C}$ . The scattering angle of  $90^{\circ}$  was used and Beckman digital correlator was intended for collecting the measured information. A thermocouple stage was used to control the temperature of ACM microgel aqueous solution precisely. Before collecting data, it should spend at least 20 min on samples making them reach an equilibrium state at the given temperature. The data was analyzed with the Delsa Nano software equipped in the computer. Under each temperature, the measurement was repeated for 3 times and the mean value of  $D_H$  was received.

#### Turbidimetric analysis

The transmittance of the ACM microgel dispersion was determined using a double beam TU-1901 Ultraviolet-visible (UV/Vis) spectrophotometer (Beijing Purkinje General Instrument Co., P.R. China) equipped with double beam. The temperature was controlled in the range from 28 to  $45\text{ }^{\circ}\text{C}$ .

#### Contact angle (CA)

The measurement process of CA was as follows. First, the slides with a size of  $20\text{ mm}\times 50\text{ mm}\times 1\text{ mm}$  were immersed in mixture solution of V(Concentrated sulfuric acid) to V(Hydrogen peroxide)=2:1 for 24 h. Then the slides were dipped into distilled water and cleaned with ultrasonic washer (Kun Shan Ultrasonic Instruments Co., People's Republic of China)

for 20 min. After that, the slides were dried completely in oven before using. Soon afterwards, 0.5 mL ACM microgel dispersions were coated on a slide in a square area of about  $2\text{ cm}\times 2\text{ cm}$  until the formation of dried film. Then the static CA of ACM microgel film was measured by a JYSP-180 contact angle meter (Jinshengxin Instrument Co., Beijing, People's Republic of China) after the film was completely dried. For reducing the error, three different experiments were conducted each group and then the average value was calculated.

#### Determination of the volume phase transition temperature (VPTT)

The VPTT was conducted on a DSC machine. Aluminum pans were used to lay sample. Approximately 10 mg of ACM microgel latexes was used under a gentle stream of nitrogen. Temperature increased from 20 to  $50\text{ }^{\circ}\text{C}$  at a heating rate of  $1\text{ }^{\circ}\text{C}/\text{min}$ . The VPTT values were determined according to the initial temperature of endothermic peak.

#### The adsorption/desorption behavior of ACM microgel to BSA

The glass bottle containing 100 mL of 6 mg/L BSA aqueous solution was first put into  $37\text{ }^{\circ}\text{C}$  water bath oscillator (Honour Instrument Co., Tianjin, P.R. China), followed by the addition of 2 mL of ACM microgel dispersion. Then, 1 mL of mixture solution was taken out each 10 min under continuous running of the oscillator. To remove the microgels in the mixture solution, Durapore PVDF filter membranes with 50 mm diameter and  $0.22\text{ }\mu\text{m}$  pore size were used (purchased from Shanghai Xinya Purifier Devices Factory). Due to the ultra low protein adsorption (protein recovery reaches 99 %) of the filter membranes to BSA, therefore, it can be thought that the BSA adsorbed by the filter membrane itself can be ignored. After filtering the solution, the residual solution was diluted to 10 mL. The absorbance of unabsorbed BSA was measured by using a double beam TU-1901 UV/Vis spectrophotometer. The wavelength of light was 280 nm and a series of three different experiments were conducted. After that the glass bottle was transferred to a shaking bath with a constant temperature of  $25\text{ }^{\circ}\text{C}$ . For the absorbance measured subsequently at  $25\text{ }^{\circ}\text{C}$ , the process was performed as above.

#### The determination of BSA absorbance

As is known, protein solution carried out on UV/Vis spectrophotometer presents the characteristic light wavelength at 280 nm [23]. Meanwhile, the absorbance value is proportional to the concentration of proteins solution. According to the

absorbance values obtained from the UV/Vis spectrophotometer, curves of the absorbance variation versus the experiment conditions could be obtained. Meanwhile, the concentration of BSA solution  $C_t$  at a certain time can be calculated according to the results showed at  $t$  time quantitatively. Finally, the BSA saturated absorbance capacity  $q$  can be easily worked out according to Eq. 1.

$$q = V_t \times \frac{C_0 - 10 \times C_t}{m_d} \times 1000 (\text{mg/g}) \quad (1)$$

Where  $C_0$  is the primary concentration of BSA aqueous solution (6 mg/L), and  $m_d$  is the weight of ACM microgel at dried state. When  $t=0$ ,  $V_t = V_0 = 200$  mL.

## Results and discussion

### The structure composition and analysis of poly(NIPAm-co-AAc-Brij-58) microgel

Figure 1 shows the FTIR spectrum of ACM microgels. As seen from Fig. 1a, characteristic adsorption peaks of amide group appear in all ACM curves. The characteristic band at  $1649 \text{ cm}^{-1}$  can be assigned to the C=O stretching of amide I band. The peak of amide II band was located at  $1546 \text{ cm}^{-1}$ , which can be ascribed to the combination of N-H bending vibrations and C-N stretching vibrations. Finally, the double peak centered at around  $1368$  and  $1387 \text{ cm}^{-1}$  was attributed to symmetrical bending vibrations and the coupling split originating from dimethyl of  $-\text{CH}(\text{CH}_3)_2$  group. From the above, it can be concluded that all curves in Fig. 1a contain the typical bands of amide group, revealing that PNIPAm has been obtained by polymerization of NIPAm monomer successfully.

It should be also known that polyNIPAm plays an important part in ACM microgel network because the mass fraction of AAc-Brij-58/NIPAm is less than 3 wt.%. Therefore, the two characteristic peaks located at  $1620$  and  $1730 \text{ cm}^{-1}$ , which assigned to the stretching vibration of  $-\text{C}=\text{C}-$  and  $-\text{O}-\text{CO}-$  groups of AAc-Brij-58 are hardly visible. Neither are the three peaks at  $1062$ – $1146 \text{ cm}^{-1}$ , which belonged to  $-\text{CH}_2-\text{O}-\text{CH}_2-$  stretching vibration. Whereas, among the magnified FTIR spectrum curves, it can be clearly seen from Fig. 1b that the peaks at  $1726 \text{ cm}^{-1}$  become gradually smoother, with the mass percentage of AAc-Brij-58/NIPAm increase from 0 to 3 wt.%. It can be attributed to the stretching vibration of C=O in  $-\text{O}-\text{CO}-$  group of AAc-Brij-58, and the slope at the point of  $1726 \text{ cm}^{-1}$  was influenced more strongly with increasing mass percentage of AAc-Brij-58/NIPAm. Therefore, it is reasonable to assume that ACM microgels have been successfully synthesized by copolymerization of AAc-Brij-58 and NIPAm.

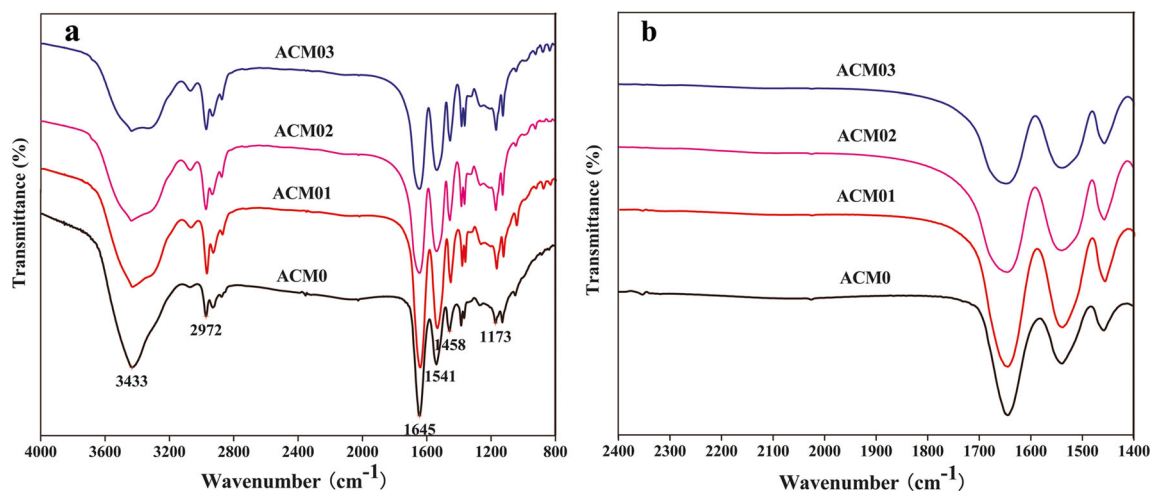
### The surface hydrophilic/hydrophobic property and morphology of poly(NIPAm-co-AAc-Brij-58) microgel

Contact angle (CA) is the significant method to investigate the hydrophilicity/hydrophobicity of the sample. Just as we all know, in smooth surface, the higher hydrophilicity leading to lower CA value. Table 1 shows the CA data and images of ACM microgel film. The CA value of the compared group measured on glass plate is  $26.8^\circ \pm 3^\circ$ , while that of ACM0, ACM01, and ACM02 microgel films are  $48.7^\circ \pm 2.8^\circ$ ,  $35.9^\circ \pm 3.6^\circ$ , and  $47.8^\circ \pm 2.9^\circ$ , respectively. In terms of ACM microgel films, the CA values are all below  $50^\circ$ . Comparing the three CA values above, it can be found that as the mass percentage of AAc-Brij-58/NIPAm is below 1 wt.%, ACM microgel film presents highest hydrophilicity. Owing to the high hydrophilic lypophilic balance (HLB) of 15.7 possessed by Brij-58, it is natural to think that the addition of AAc-Brij-58 leads to the formation of hydrogen bond between hydrophilic PEO groups of AAc-Brij-58 and water molecules. This result is in good agreement with previous findings reported by Zhang et al. [24]. The subsequent increase of CA value for ACM microgels film can be attributed to the dominant role played by the hydrophobic ester groups and  $-\text{C}_{16}\text{H}_{33}$  groups in polyAAc-Brij-58 molecular chains. In fact, the CA results have been proved by the following measurements like TEM, DLS, and UV/Vis.

The morphology of ACM microgel particles is presented in Fig. 2. It can be seen that all the ACM microgel particles present spherical structure and narrow particle size distribution except ACM03. Roughly calculated, it was found that the microgel diameters of ACM0, ACM01, and ACM02 were about 580, 900 and 400 nm, respectively. As a matter of fact, during the polymerization reaction, the increasing addition of ester surfactant AAc-Brij-58 would facilitate the formation of AAc-Brij-58 micelles. Blandamer et al. [25] have pointed out that the concentration of surfactant above the so-called critical micelle concentration (CMC) will lead to the formation of micelles. As the free-radical reaction proceeded, part of ester chains in poly(NIPAm-co-AAc-Brij-58) network grew to a certain length and became insoluble in water, which gradually led to the reversed-phase precipitation of molecular chains and the formation of ACM microgel particles in aqueous solution.

Furthermore, with increasing mass percentage of AAc-Brij-58/NIPAm from 0 to 2 wt.%, the  $D_H$  of ACM0, ACM01, and ACM02 microgels at  $28^\circ \text{C}$  can be roughly gained as 928, 1100, and 760 nm, respectively. This variation tendency of  $D_H$ , which increases firstly and then decreases can be explained by the following two competitive effects. On one hand, the introduction of AAc-Brij-58 with hydrophobic groups of  $-(\text{CH}_2)_{15}\text{CH}_3$  and hydrophilic groups of  $-(\text{CH}_2\text{CH}_2\text{O})_{20}\text{OH}$  certainly increases  $D_H$  of PNIPAm chains. On the other hand, owing to the relatively enhanced



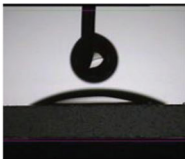
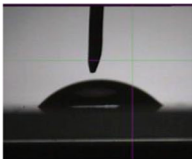
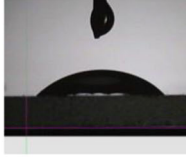

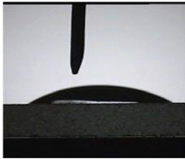
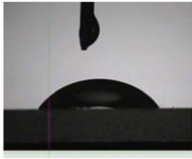
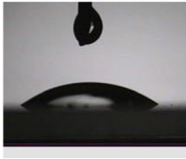
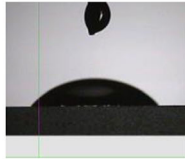
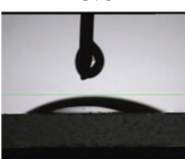
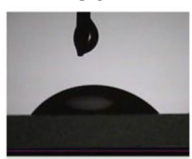
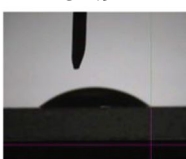
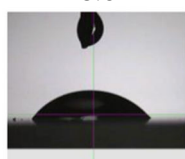


**Fig. 1** The FTIR spectrum of ACM microgel (a) and the FTIR spectrum of ACM0-03 microgel (b). The locally enlarged image with the wavenumber range of 2400–1400  $\text{cm}^{-1}$

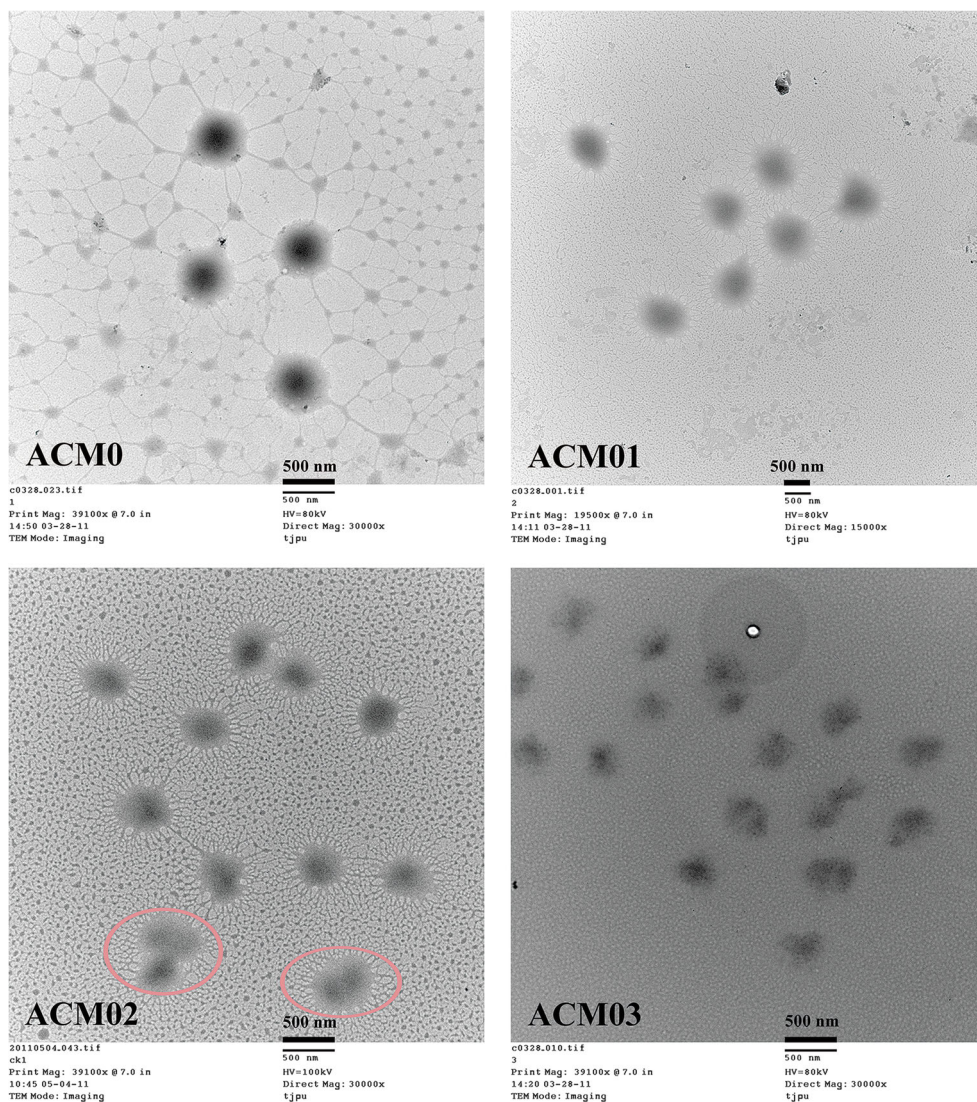
hydrophobic effect,  $D_H$  of ACM microgels decrease. It is evident from the circle marked picture of ACM02 that a small portion of ACM02 microgel particles aggregated. It indicates that hydrophobic effect plays a significant role in the size of ACM microgel particles, as the mass percentage of AAc-Brij-

58/NIPAm increases from 1 wt.% to 2 wt.%. The change of hydrophilicity/hydrophobicity for ACM microgel has been confirmed by the CA measurement above. As a matter of fact, Farn et al. [26] have pointed out that, in terms of amphiphilic surfactant, both the solubility of hydrophobic group in

**Table 1** The surface CA values of glass plate and ACM microgel films

The surface CA values of glass plate and ACM microgel films				
groups	glass plate	ACM0	ACM01	ACM02
1	27.1° 	45.5° 	39.8° 	50.2° 
2	24.7° 	50.6° 	32.9° 	44.5° 
3	28.6° 	50° 	34.9° 	48.6° 
average value	26.8°±3°	48.7°±2.8°	35.9°±3.6°	47.8°±2.9°

**Fig. 2** The TEM images of ACM microgels



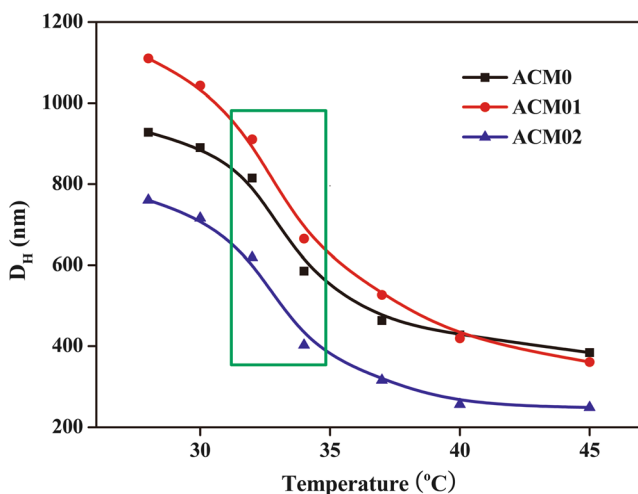
aqueous solution and the hydrophilic group in nonpolar phase are very low and therefore the formation of aggregates depending on hydrophobic effect.

As the mass percentage of AAC-Brij-58 reaches 3 wt.%, the hydrophobic effect of ACM03 microgel is the most remarkable. As a result, irregular shapes of ACM03 microgel particles can be observed. In fact, during the polymerization of ACM03, explosive reaction occurred and followed by the generation of solid particles. Based on this matter, the subsequent measurement related to ACM03 microgel won't be analyzed or clarified.

#### Thermo-sensitivity of poly(NIPAm-co-AAC-Brij-58) microgel

Hirokawa et al. [27] have pointed out that PNIPAm molecular chains exhibit significantly temperature sensitivity, owing to the hydrophilic amide groups and the hydrophobic isopropyl

groups in molecular chains. Meanwhile, because of an obvious hydrophilicity/hydrophobicity change around VPTT, PNIPAm-based microgels generally present rapid sensitivity to temperature. The temperature-sensitivity of microgels can be easily confirmed by DLS, upon which the  $D_H$  curve of microgel spheres as a function of temperature or VPTT can be obtained. Figure 3 shows the particle size variation of ACM microgels as a function of temperature. It can be found that the  $D_H$  values of ACM0, ACM01, and ACM02 decrease to 384, 360, and 248 nm from 928, 1100, and 760 nm, with increasing temperature from 28 °C to 45 °C, respectively. Significant decrease upon  $D_H$  can be observed between 32 and 34 °C. It indicates that all ACM microgels exhibit good thermo-responsibility, regardless of the mass percentage of AAC-Brij-58/NIPAm. On the other hand, it also shows that the VPTT values of ACM microgels mainly occur at 32–34 °C. To further investigate the effect of addition of AAC-Brij-58 upon thermo-responsibility of ACM microgels, in

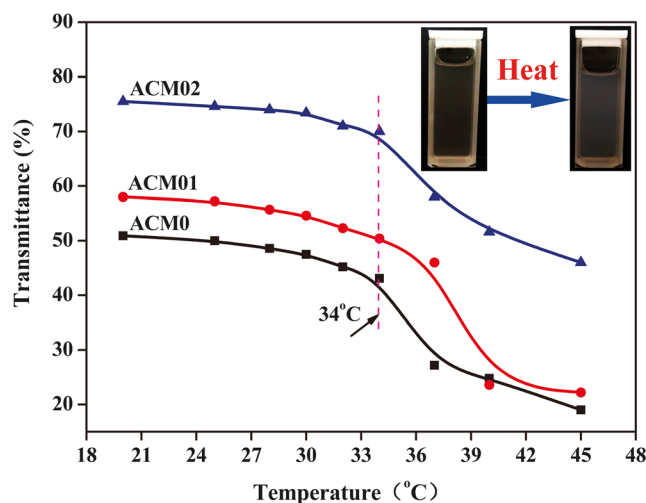


**Fig. 3** Plots of  $D_H$  versus temperature for the ACM microgels

Fig. 3 the positive slope values of ACM microgels between 32 and 34 °C are calculated. For ACM0, ACM01, and ACM02 microgels, the values obtained are 114.85, 122.8, and 108.05, respectively. The slope values demonstrate that the sensitivity of ACM01 microgels in response to temperature is much better than those of ACM0 and ACM02.

It is also noteworthy that below 40 °C, the relationship among the  $D_H$  values of ACM microgels shows that  $ACM01 > ACM0 > ACM02$ , which is in good agreement with the results of Fig. 2. It reconfirmed that as the mass percentage of AAc-Brij-58/NIPAm is below 1 wt.%, the hydrophilicity of ACM microgels increases. While as the mass percentage of AAc-Brij-58/NIPAm is above 1 wt.%, the hydrophilicity of ACM microgels decreases. It is interesting to note that, when the temperature is above 40 °C, the  $D_H$  values of ACM01 are less than ACM0. The reason is considered to be that the higher temperature leads to the destruction of hydrogen bonds, the hydrophobic effect of alkyl groups in AAc-Brij-58 plays a dominant role in microgel emulsion. As a result, the hydrophobic state results in the bigger loss of water in ACM01 microgels and the microgels shrink. This can be aided by the report of Ricka et al. [28].

UV/Vis method was also adopted to analyze the thermo-responsibility of ACM microgels. The varied transmittance curves of ACM microgels versus temperature are shown in Fig. 4. It can be seen that the transmittance of ACM microgels decrease gradually as temperature increases from 28 °C to 45 °C. The illustration shown in Fig. 4 also shows that with the temperature increase, the appearance of ACM microgel latex turns to ivory from transparency, confirming the thermo-responsibility of ACM microgels from macroscopic appearance. The varied transmittance of ACM microgel latex is mainly due to the water existing in the interior void of microgels, which reveals the difference value of refractive index between water-microgel macrocomplex and bulk water.

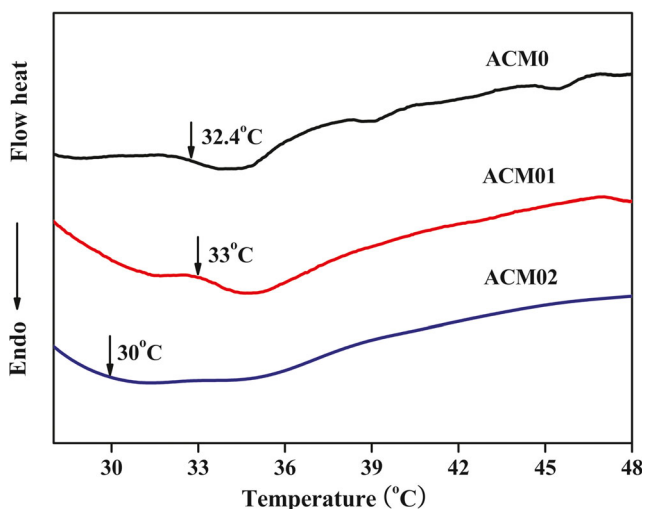


**Fig. 4** Curves of the transmittance variation of the ACM microgel dispersions versus temperature

Below VPTT, the difference in the refractive index is small by virtue of swollen state of microgels, resulting in a higher transmittance. However, as temperature above VPTT, ACM microgels become curly hard spheres from previous stretching network. As a result, as Pelton et al. [29] have proved, water was expelled from the interior of microgels, leading to a higher refractive index and a lower transmittance. Furthermore, it is of interest to note that the transmittance of ACM microgels rapidly decreased at ca. 34–36 °C, slightly higher than those achieved from Fig. 3. The reason may be attributed to the hysteresis effect generated by the fact that the real temperature in the heating bath is actually lower than the digital display. It is also worth noting that the VPTT of ACM01 is higher than that of other two groups. This result confirms again that the hydrophilicity of ACM microgels decreases after originally increases with increasing mass percentage of AAc-Brij-58/NIPAm from 0 to 2 wt.%, which is in good accordance with the result in Fig. 3 and Table 1.

DLS and UV/Vis methods can only provide a broad scope of VPTT. In order to investigate the fixed VPTT value, DSC was used to determine VPTT of ACM microgel, as shown in Fig. 5. It can be seen that all DSC curves of ACM microgel dispersions present weak endothermic peak. This is because that ACM microgel latex contains large amounts of water, and the volume changes of ACM microgels are not obvious like bulk hydrogel that was reported by Gao et al. [30]. Despite this special issue, the endothermic peaks can still be found from DSC curves of ACM microgel after magnification. It shows that the VPTT values (the starting point of the peaks) of ACM0, ACM01, and ACM02 microgel dispersions are 32.4, 33, and 30 °C, respectively. It is known that in the heating process of DSC, the hydrogen bonds between water molecules and hydrophilic groups of microgels are destroyed due to the energy absorption, causing water to be expelled from microgel interior. The more water is excluded, the more





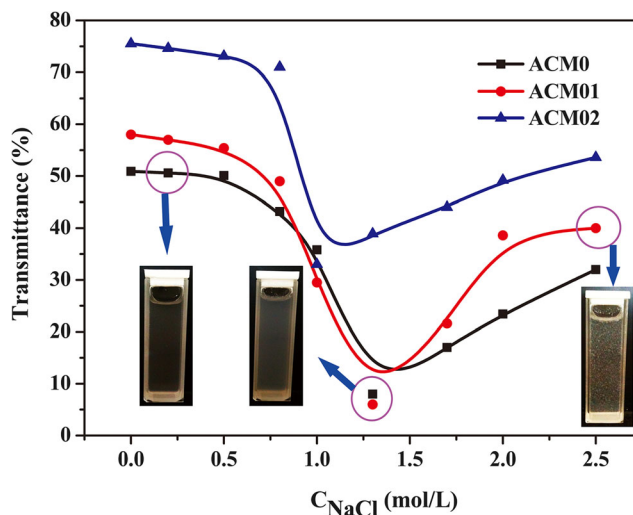
**Fig. 5** DSC curves of ACM microgels

energy will be consumed, and the more obvious endothermic peaks in the DSC curve will appear. For ACM02 microgel, less energy was needed to consume for the deswelling process by virtue of the lower hydrophilicity, leading to the formation of very weak endothermic peak. In fact, high hydrophilicity would increase the VPTT of gels. Fernandez et al. [31] and Bradley et al. [32] have confirmed it by introducing hydrophilic group AAC in polymer and observed the increase of VPTT. Conversely, high hydrophobicity of copolymer leads to the VPTT decreases.

#### The stability of poly(NIPAm-co-AAc-Brij-58) microgel under salt stimulus

In medicine, cosmetics, and other fields, the practical application of the intelligent microgel closely relates to its stability. It is normally required that microgel should be stable within a certain range of ionic strength and temperature. It is well known that the stability of colloid is decided by the van der Waals force, electrostatic repulsion, and spatial stability. And the separation, aggregation, and sedimentation of the colloid occur as the van der Waals force is greater than the electrostatic repulsion and spatial stability [33, 34].

The transmittance change curves of the ACM microgel dispersions versus different concentrations of NaCl solution are shown in Fig. 6. It is seen that with the increase of NaCl concentration, the transmittance of ACM microgel emulsion decreases at the beginning and then increases. As the concentrations of NaCl are 1.42, 1.35, and 1.12 mol/L, respectively, the minimal transmittance values of ACM microgel emulsion were reached. And these points are denoted as the critical salt concentration point of the microgel aggregation, above which the ACM microgel particles would aggregate immediately, followed by the gradually increase of light transmittance. As is known to all, there are two main reasons that the NaCl



**Fig. 6** The transmittance change curves of the ACM microgel dispersions versus different concentrations of NaCl solution

solution system destroys the stability of microgel [35, 36]. One is that the electrostatic repulsion is shielded by the introduction of NaCl, and the shielding effect is enhanced with the increase of NaCl concentration, leading to the electrostatic repulsion decreases. The other is that the osmotic pressure inside and outside the microgel particles are different on account of the addition of NaCl. As a result, the water inside the particles penetrate outward continuously, causing particle size decreases, indicating that the original stability of particle size is gradually lost. With increasing NaCl concentration, the microgel emulsion turned to turbid from transparent with the gradually precipitation of the subtle solid particle, until it reached an ultimate transparent emulsion followed by the sedimentation of the solid particle. Consequently, the light transmittance originally reduces and then increases with the increase of NaCl concentration. It is also interesting to note that along with the mass percentage of AAC-Brij-58/NIPAm increasing, the critical point decreased because of polar groups in AAC-Brij-58, which means the sensitivity that the system of ACM microgel reacted to ionic strength increased. Meanwhile, introduction of NaCl to the suspension induced the “salt-out” effect of ACM microgel, leading to the dehydration of poly(NIPAm) chains in microgel network, therefore the shrinkage of microgel was produced [37]. Moreover, with the increase of NaCl concentration, the osmotic pressure in solution was higher than that in the microgel network. Therefore, water was released from the inside of microgel, reducing the  $D_H$  of microgel particle [38]. This also can be explained by the hairy layer model, which has been elucidated by Seebergh et al. [39]. The model holds that microgel network is composed of many polymer chains, or hairs, they extend into the surrounding solution due to the electrostatic repulsion between charged groups in polymer chains. The electrostatic repulsion is screened by the presence of NaCl, resulting in the decrease of hairy layer thickness. Therefore, the  $D_H$  of

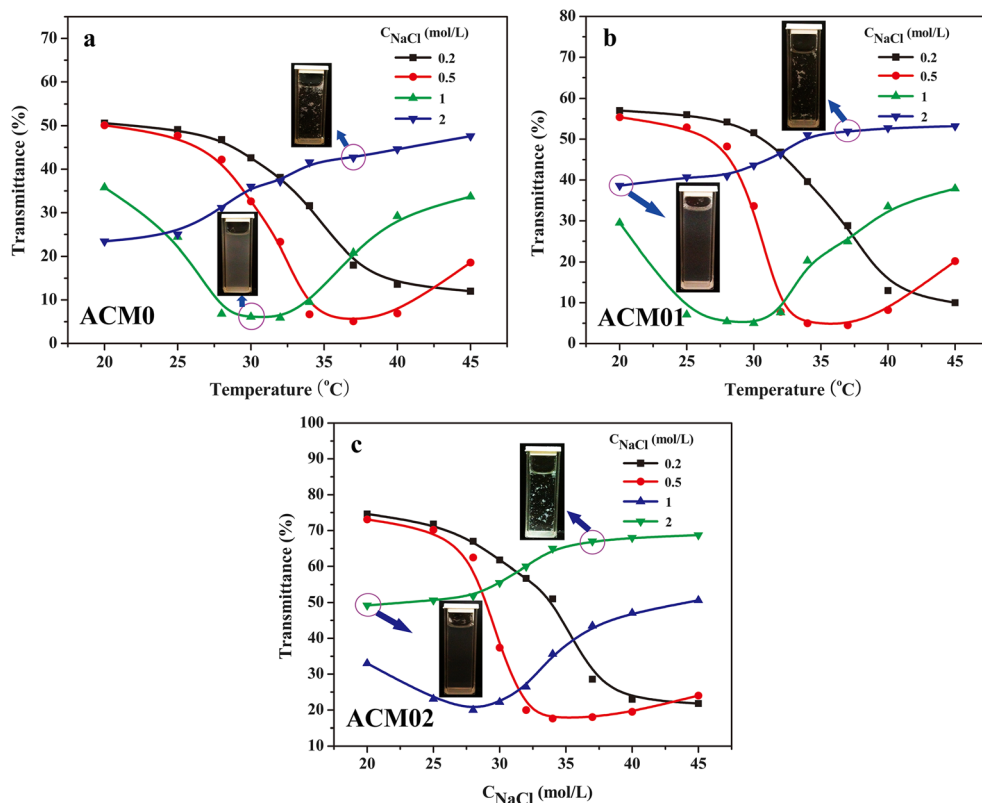


microgel particle decreases. Furthermore, dehydration of ACM microgel results in the value of effective Hamaker constant ( $A_{\text{eff}}$ ) increased, and the spatial stability of ACM microgel system was damaged simultaneously. These worked together to generate the formation of aggregates [40]. In terms of ACM02, owing to the self-aggregation of ACM02, the needed critical aggregation salt concentration decreased.

Taking thermo-responsibility and salt-sensitivity of ACM microgels into consideration together, the stability of ACM microgels versus temperature under different salt concentrations are shown in Fig. 7. Taking the critical aggregation salt concentration as points of separation, the thermal stability of ACM microgels under 0.2, 0.5, 1.0, and 2.0 mol/L NaCl solution was investigated. It is well known that destroying the stability of microgel emulsion by means of increasing temperature mainly stems from following two reasons [11, 41]. One is that the particle sizes gradually decrease with the increasing of temperature, and the steric stability disappears progressively. Secondly, the thermal motion of microgel particles in higher temperature is more drastic, at higher temperature the collision likelihood of particles improves; therefore, it is easier for the aggregation of microgel particles. Figure 7a–c show that in 0.2 mol/L NaCl solution, the transmittance values of ACM microgel dispersions drop markedly as the temperature is above VPTT, and then keep slightly decreasing. It indicates that heating can not induce the aggregation of ACM microgel

particles when the concentration of NaCl solution is below 0.2 mol/L. However, when the concentration of NaCl solution reaches 0.5 mol/L, some solid particles appear owing to the self-aggregation of microgel dispersions. Moreover, it becomes easier for the solid particles to aggregate with the increase of temperature. It turns out that the increase of NaCl concentration and temperature both make the transmittance of microgel latex reduce sharply, and the sudden decrease appears below the phase transition temperature. The reason is that both the improvement of the ion strength and the increase of temperature promote water expelled from microgels, which can increase the difference of refractive indices between water and microgels [7]. Whereas the transmittance will increase on the condition that continues to heat up afterwards, it can be attributed to the aggregation of solid particles. When the concentration of NaCl is 1 mol/L, the transmittance curve is similar to that of 0.5 mol/L NaCl solution, somewhat differently, the abrupt change point of temperature is lower due to the increased concentration of NaCl. As the concentration of NaCl is 2 mol/L, aggregates appeared in ACM microgel dispersions. In the wake of increase in temperature, microgels aggregated more severely and the transmittance increased accordingly. In addition, a sudden change appeared around the phase transition temperature. It demonstrates that the aggregation behavior was aggravated with the particle size of microgel decreased and the spatial stability disappeared, which led to the increase of transmittance values.

**Fig. 7** The transmittance change curves of the ACM microgel dispersions versus temperature in NaCl solution (a), the transmittance change curves of the ACM0 microgel dispersions versus temperature at 0.2, 0.5, 1, and 2 mol/L NaCl solution, respectively (b), and the transmittance change curves of the ACM0 microgel dispersions versus temperature at 0.2, 0.5, 1, and 2 mol/L NaCl solution, respectively (c). The transmittance change curves of the ACM0 microgel dispersions versus temperature at 0.2, 0.5, 1, and 2 mol/L NaCl solution, respectively



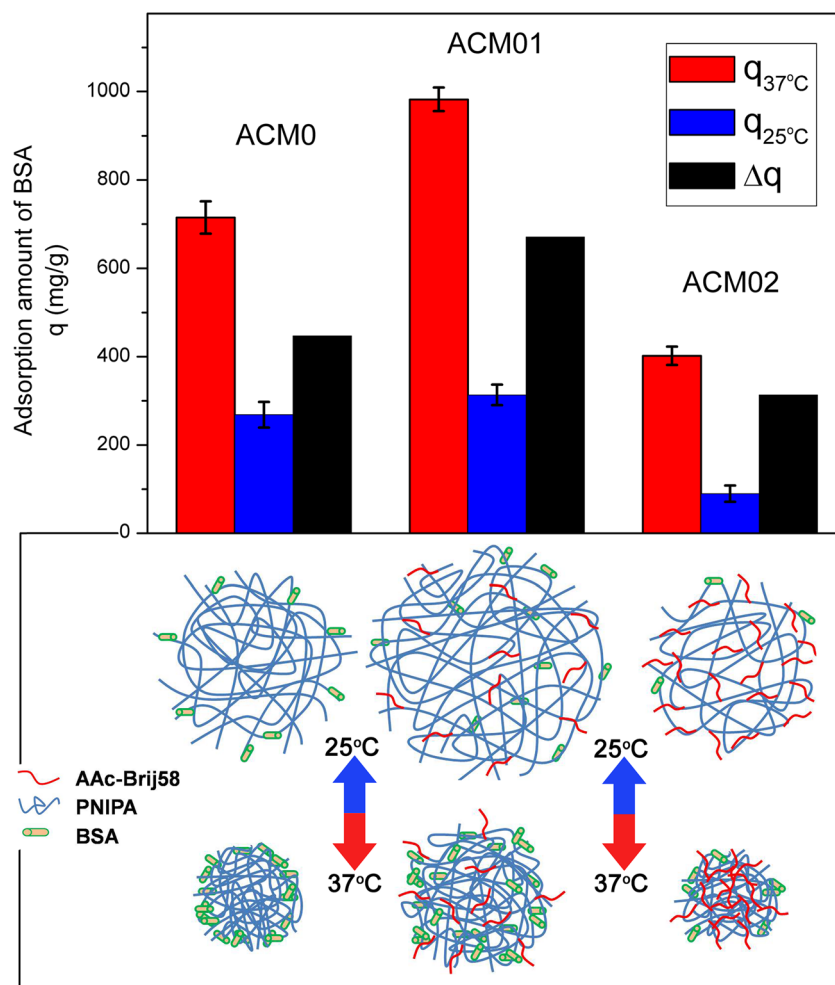
### The adsorption/desorption behavior of ACM microgel onto BSA

The column diagram of BSA adsorption content and the schematic illustration of BSA adsorption/desorption onto ACM0-02 microgels at 25 °C and 37 °C are shown in Fig. 8. It was found that both the BSA adsorption amount at 25 or 37 °C and the adsorption difference between 37 °C and 25 °C showed a trend that increase first and then decrease. For instance, the BSA adsorption amounts of ACM0, ACM01, and ACM02 are  $714.7 \pm 36$ ,  $982.7 \pm 26$  and  $402 \pm 20$  mg/g, respectively. In our previous work, it was proved that as mass percent of AAc-Brij-58/NIPAm was 1 wt.%, poly(NIPAM-*co*-AAc-Brij-58) (ACH01) bulk hydrogel presented the highest adsorbed BSA amount, which was about  $1090 \pm 24$  mg/g at 37 °C. And no BSA aggregates on the surface of ACH hydrogels were observed after desorption at 25 °C [20]. Similar to ACH hydrogel, in the process of microgel collapse, polyAAc-Brij-58 plays an extremely important role in the BSA adsorption/desorption. Owing to the hydrophobic alkyl chains  $-C_{16}H_{33}$  in polyAAc-Brij-58, they promote BSA to be adsorbed easily. Conversely, the electrostatic repulsion of ethoxy groups in

AAc-Brij-58 would cause negative impact on BSA adsorption.

Figure 3 shows that the particle size of ACM01 is bigger than ACM0 within the range of 25 to 40 °C. Therefore, in the phase transition process of BSA adsorption from 25 to 37 °C, it will be easier for BSA to penetrate into the network structure of ACM01 microgel and adsorbed at the external and central section, as illustrated in Fig. 8b. It can be explained from the fact that the bigger the particle size is, the larger adsorption area will be. Combining this with the promoting adsorption effect of AAc-Brij-58 mentioned above, a larger amount of BSA adsorption onto ACM01 than ACM0 microgel ultimately realized at 37 °C. On the other hand, although the electrostatic repulsion of ethoxy groups in AAc-Brij-58 promoted BSA desorption in the ACM01 surface layer at 25 °C, the promoting adsorption effect of AAc-Brij-58 plays a dominate role in BSA adsorption, hence the adsorption amount of BSA onto ACM01 microgel is still larger than ACM0. It probably can be attributed to the fact that some BSA macromolecules are tangled in the central and external section of microgels; therefore, the movement of tangled BSA is restricted by the poly(NIPAM-*co*-AAc-Brij-58) molecular chains. From the

**Fig. 8** The bar chart of BSA adsorption quantity and the schematic illustration of BSA adsorption/desorption at different temperatures



difference values of adsorption it can be concluded that the adsorption effect improved by ACM01 is more significant than ACM0.

With increasing mass percentage of AAc-Brij-58/NIPAm from 1 wt.% to 2 wt.%, the particle size of ACM02 becomes smaller at 25 °C and the effective adsorption area reduces. Meanwhile, various structures of AAc-Brij-58 appear and the steric hindrance effect is more prominent with the increase of mass percentage. All these work together to strengthen the ability of anti-adsorption to BSA, thus the adsorption amounts of BSA onto ACM02 at 25 °C and 37 °C all eventually reach the minimum value than ACM0 and ACM01.

On the other hand, in virtue of the introduction of AAc-Brij-58, the electrostatic repulsive effect of  $-\text{CH}_2-\text{CH}_2-\text{O}$ -groups to BSA is more highlighted in ACM microgels than in poly(NIPAm-*co*-AAc-Brij-58) (ACHX) bulk hydrogel. In consequence, the adsorption/desorption behavior of BSA onto ACM0 is improved apparently compared to ACHX bulk hydrogel. While, as for ACM01 and ACM02, only the desorption performance onto BSA increased.

## Conclusions

In the present work, a series of poly(NIPAm-*co*-AAc-Brij-58) (ACM) microgels with various mass percentages of AAc-Brij-58/NIPAm were successfully synthesized by aqueous precipitation polymerization. With the diameter ranges from 400 to 900 nm, all of the ACM microgel particles obtained present spherical shape and narrow particle size distribution. Increasing the mass percentage of AAc-Brij-58/NIPAm from 0 to 2 wt.%, the obtained CA values of ACM0, ACM01, and ACM02 film are  $48.7^\circ \pm 2.8^\circ$ ,  $35.9^\circ \pm 3.6^\circ$  and  $47.8^\circ \pm 2.9^\circ$ , respectively. The obtained ACM microgels present rapid temperature- and salt-responsibility. The  $D_H$  values of ACM0, ACM01, and ACM02 microgels from 928, 1100, and 760 nm decrease to 384, 360, and 248 nm separately as temperature increases from 28 °C to 45 °C. With the increase of NaCl concentration from 0 to 2.5 mol/L, the transmittance value of ACM microgel emulsion decreases initially and increases afterwards. As ACM0-02 microgel aggregate, accordingly, the critical salt concentration is 1.42, 1.35, and 1.12 mol/L, respectively. However, with the temperature increasing at a certain NaCl concentration, there were no aggregations below 0.2 mol/L. However, above 0.5 mol/L, the stability of ACM microgels was destroyed. The adsorption amounts of BSA onto ACM0, ACM01, and ACM02 microgel dispersions are  $714.7 \pm 36$ ,  $982.7 \pm 26$  and  $402 \pm 20$  mg/g, respectively. Meanwhile, with the maximum adsorption difference value of 670 mg/g, ACM01 shows great potential applications in drug release and delivery in vivo.

**Acknowledgments** This work has been supported by Science and Technology Correspondent of Tianjin (14JCTPJC00502 and 15JCPJC62200), Science and Technology Planning Project of Shandong Provincial Education Department (J06K63), and National Training Programs of Innovation and Entrepreneurship for Undergraduates (201510058005 and 201510058051), and the grant from the Applied Basic Research and Advanced Technology Programs of Science, Technology Commission Foundation of Tianjin (12JCQNJC01400 and 15JCYBJC18300), the State Scholarship Fund of China Scholarship Council (201508120037), and Tianjin Polytechnic University Innovation for Postgraduate (15108).

## Compliance with ethical standards

**Conflict of interest** The authors declare that they have no competing interests.

## References

1. Pelton RH, Chibante P (1986) Preparation of aqueous lattices with *N*-isopropylacrylamide. *Colloid Surf* 20:247–256
2. Todd H, Robert P (2008) Impact of microgel morphology on functionalized microgel-drug interactions. *Langmuir* 24:1005–1012
3. Masoud H, Alexeev A (2012) Controlled release of nanoparticles and macromolecules from responsive microgel capsules. *ACS Nano* 6:212–219
4. Gawlitza K, Georgieva R, Tavraz N, Keller J, Klitzing RV (2013) Immobilization of water-soluble HRP within poly-*N*-isopropylacrylamide-microgel particles for use in organic media. *Langmuir* 29:16002–16009
5. Tripathi BP, Dubey NC, Stamm M (2014) Hollow microgel based ultrathin thermoresponsive membranes for separation, synthesis, and catalytic applications. *Appl Mater Interfaces* 6:17702–17712
6. Faccia PA, Pardini FM, Amalvy JI (2015) Evaluation of pH-sensitive poly(2-hydroxyethyl methacrylate-*co*-2-(diisopropylamino)ethyl methacrylate) copolymers as drug delivery systems for potential applications in ophthalmic therapies/ocular delivery of drugs. *Expr Polym Lett* 9:554–566
7. Zhang QS, Zha LS, Ma JH, Liang BR (2007) Synthesis and characterization of novel, temperature-sensitive microgels based on *N*-isopropylacrylamide and tert-butyl acrylate. *J Appl Polym Sci* 103:2962–2967
8. Zhang WJ, Mao ZW, Gao CY (2014) Preparation of TAT peptide-modified poly(*N*-isopropylacrylamide) microgel particles and their cellular uptake, intracellular distribution, and influence on cytotoxicity in response to temperature change. *J Colloid Interface Sci* 434:122–129
9. Hou W, Shen YH, Liu HM, Zhang AQ, Dai S (2014) Mechanical properties of pH-responsive poly(2-hydroxyethyl methacrylate/methacrylic acid) microgels prepared by inverse microemulsion polymerization. *React Funct Polym* 74:101–106
10. Klinger D, Landfester K (2011) Photo-sensitive PMMA microgels: light-triggered swelling and degradation. *Soft Matter* 7:1426–1440
11. Duracher D, Elaissari A, Pichot C (1999) Characterization of cross-linked poly(*N*-isopropylacrylamide) microgel latexes. *Colloid Polym Sci* 277:905–913
12. Chen GX, Liu JX, Yang YD, Zhang LJ, Wu M, Ni HM (2015) Preparation of pH-sensitive nanoparticles of poly(methacrylic acid) (PMAA)/poly(vinyl pyrrolidone) (PVP) by ATRP-template miniemulsion polymerization in the aqueous solution. *Colloid Polym Sci* 293:2035–2044

13. Zhou XJ, Nie JJ, Wang Q, Du BY (2015) Thermosensitive ionic microgels with pH tunable degradation via in situ quaternization cross-linking. *Macromolecules* 48:3130–3139
14. Zheng XW, Qian JC, Tang F, Wang ZR, Cao CY, Zhong K (2015) Microgel-based thermosensitive MRI contrast agent. *ACS Macro Lett* 4:431–435
15. Gan TT, Zhang YJ, Guan Y (2009) In situ gelation of P(NIPAM-HEMA) microgel dispersion and its applications as injectable 3D cell scaffold. *Biomacromolecules* 10:1410–1415
16. Sow LC, Yang HS (2015) Effects of salt and sugar addition on the physicochemical properties and nanostructure of fish gelatin. *Food Hydrocolloids* 45:72–82
17. Nolan CM, Reyes CD, Debord JD (2005) Phase transition behavior, protein adsorption, and cell adhesion resistance of poly(ethylene glycol) cross-linked microgel particles. *Biomacromolecules* 6:2032–2039
18. Silva CSO, Baptista RP, Santos AM, Martinho JMG, Cabral JMS, Taipa MA (2006) Adsorption of human IgG on to poly(*N*-isopropylacrylamide)-based polymer particles. *Biotechnol Lett* 28:2019–2025
19. Trongsatitkul T, Budhlall BM (2013) Temperature dependence of serum protein adsorption in PEGylated PNIPAm microgels. *Colloids Surf B: Biointerfaces* 103:244–252
20. Liu PF, Gao WJ, Zhang QS, Chen K, Zhang J, Chen L, Zhang XY, Wang K (2015) Temperature-sensitive hydrogel modified by polymerizable liquid crystal AAc-Brij-58: optical and protein adsorption/desorption behaviors. *React Funct Polym* 89:1–8
21. Jones CD, Lyon LA (2000) Synthesis and characterization of multiresponsive core-shell microgels. *Macromolecules* 33:8301–8306
22. Pelton R (2000) Temperature-sensitive aqueous microgels. *Adv Colloid Interf Sci* 85:1–33
23. Coulter CB, Stone FM, Kabat EA (1936) The structure of the ultraviolet absorption spectra of certain proteins and amino acids. *J Gen Physiol* 19:739–752
24. Zhang QS, Peng Z, Zhang K, Chen L, Zhao YP (2013) Effect of hydrophilic segment length of liquid crystal templates on the morphology and thermal responsibility of hydrogels. *Acta Polym Sin* 7:841–848
25. Blandamer MJ, Cullis PM, Engberts JBFN (1996) Calorimetric studies of macromolecular aqueous solutions. *Pure Appl Chem* 68:1577–1582
26. Farn RJ (2006) Chemistry and technology of surfactants. Blackwell Publishing, Oxford
27. Hirokawa Y, Tanaka T (1984) Volume phase transition in a nonionic gel. *J Chem Phys* 81:6379–6380
28. Ricka J, Tanaka T (1984) Swelling of ionic gels: quantitative performance of the donnan theory. *Macromolecules* 17:2916–2921
29. Pelton RH, Pelton HM, Rowell RL, Morphesis A (1989) Particle sizes and electrophoretic mobilities of poly(*N*-isopropylacrylamide) latex. *Langmuir* 5:816–818
30. Gao WJ, Zhang QS, Liu PF, Zhang SH, Zhang J, Chen L (2014) Trail of pore shape and temperature-sensitivity of poly(*N*-isopropylacrylamide) hydrogels before and after removing Brij-58 template and pore formation mechanism. *RSC Adv* 4:34460–34469
31. Fernandez-Nieves A, Fernandez-Barbero A, Vincent B, de las Nieves FJ (2000) Charge controlled swelling of microgel particles. *Macromolecules* 33:2114–2118
32. Bradley M, Ramos J, Vincent B (2005) Equilibrium and kinetic aspects of the uptake of poly(ethylene oxide) by copolymer microgel particles of *N*-isopropylacrylamide and acrylic acid. *Langmuir* 21:1209–1215
33. Duracher D, Sauzedde F, Elaissari A, Nabzar L (1998) Cationic amino-containing *N*-isopropylacrylamide-styrene copolymer particles: surface and colloidal characteristics. *Colloid Polym Sci* 276:920–929
34. Rasmusson M, Routh A, Vincent B (2004) Flocculation of microgel particles with sodium chloride and sodium polystyrene sulfonate as a function of temperature. *Langmuir* 20:3536–3542
35. Zhu PW, Napper DH (1995) The effects of different electrolytes on the fractal aggregation of polystyrene latexes coated by polymers. *Colloids Surface A* 98:93–106
36. Deng YL, Xiao HN, Pelton R (1996) Temperature-sensitive flocculants based on poly (*N*-isopropylacrylamide-*co*-diallyldimethylammonium chloride). *J Colloid Interface Sci* 179:188–193
37. Daly E, Saunders BR (2000) Temperature-dependent electrophoretic mobility and hydrodynamic radius measurements of poly(*N*-isopropylacrylamide) microgel particles: structural insights. *Phys Chem Chem Phys* 2:3187–3193
38. Zha LS, Hu JH, Wang CC, Fu SK, Luo MF (2002) The effect of electrolyte on the colloidal properties of poly(*N*-isopropylacrylamide-*co*-dimethylaminoethylmethacrylate) microgel latexes. *Colloid Polym Sci* 280:1116–1121
39. Seebergh JE, Berg JC (1995) Evidence of a hairy layer at the surface of polystyrene latex particles. *Colloids Surf* 100:139–153
40. Emma D, Brian RS (2000) A Study of the effect of electrolyte on the swelling and stability of poly(*N*-isopropylacrylamide) microgel dispersions. *Langmuir* 16:5546–5552
41. Garcia-Salinas MJ, Romero-Cano MS, de las Nieves FJ (2002) Colloidal stability of a temperature-sensitive poly(*N*-isopropylacrylamide/2-acrylamido-2-methylpropanesulphonic acid) microgel. *J Colloid Interface Sci* 248:54–61